environments

MDPI

Article

The Formation and Stability of HA–Fe/Mn Colloids in Saturated Porous Media

Junhao Zheng [1], Mei Jiang [1], Qingzhu Li [1,2] and Weichun Yang [1,2,*]

[1] School of Metallurgy and Environment, Central South University, Changsha 410083, China; 203501048@csu.edu.cn (J.Z.); 233512175@csu.edu.cn (M.J.); qingzhuli@csu.edu.cn (Q.L.)
[2] Chinese National Engineering Research Center for Control & Treatment of Heavy Metal Pollution, Changsha 410083, China
* Correspondence: yang220@csu.edu.cn

Abstract: Fe/Mn (hydr)oxides are metallic compounds that exhibit significant redox activity in environmental media and play a pivotal role in geochemical processes, thereby influencing the fate of metals in porous media. The morphology of Fe/Mn (hydr)oxides in natural environments and their interactions with trace metals are significantly influenced by the presence of natural organic matter (NOM). However, there is limited understanding regarding the formation, transport, and stability of Fe/Mn (hydr)oxides in the environment. The present study employed humic acid (HA) as a representative NOM material to investigate the positive influence of HA on the formation of Fe/Mn colloids. However, there remains limited comprehension regarding the formation, transport, and stability of Fe/Mn (hydr)oxides in the natural environment. In this study, we investigated the positive effect of natural organic matter (NOM) on the formation of Fe/Mn colloids using humic acid (HA) as a representative NOM material. We comprehensively characterized the chemical and physical properties of HA–Fe/Mn colloids formed under various environmentally relevant conditions and quantitatively analyzed their subsequent aggregation and stability behaviors. The findings suggest that the molar ratios of C to Fe/Mn (hydr)oxide play a pivotal role in influencing the properties of HA–Fe/Mn colloids. The formation and stability of HA–Fe/Mn colloids exhibit an upward trend with increasing initial molar ratios of C to Fe/Mn. Redox and metal–carboxylic acid complexation reactions between HA and hydrated iron/manganese oxides play a pivotal role in forming colloidal HA–Fe/Mn complexes. Subsequent investigations simulating porous media environments have demonstrated that the colloidal structure resulting from the interaction between HA and Fe/Mn facilitates their migration within surrounding porous media while also enhancing their retention in the surface layers of these media. This study offers novel insights into the formation and stabilization mechanisms of HA–Fe/Mn colloids, which are pivotal for comprehending the behavior of Fe/Mn colloids and the involvement of Fe/Mn (hydr)oxides in geochemical cycling processes within porous media.

Keywords: natural organic matter; humic acid; Fe/Mn (hydr)oxides; HA–Fe/Mn colloids; colloid formation; stability

Citation: Zheng, J.; Jiang, M.; Li, Q.; Yang, W. The Formation and Stability of HA–Fe/Mn Colloids in Saturated Porous Media. *Environments* **2024**, *11*, 136. https://doi.org/10.3390/environments11070136

Academic Editors: Erich Wieland and Claude Fortin

Received: 27 April 2024
Revised: 22 June 2024
Accepted: 24 June 2024
Published: 27 June 2024

1. Introduction

Global concern over the accumulation of heavy metal ions (HMs) in the soil and groundwater resulting from anthropogenic industrial activities has been the subject of significant scholarly attention in recent decades [1–3]. Significantly, the co-occurrence of arsenic, cadmium, and lead contamination is particularly severe in regions associated with metal mining, smelting operations, metal processing facilities, and areas irrigated with sewage [4–6]. Iron/manganese hydroxide and oxide mixtures (Fe/Mn (hydr)oxides) are widely present in natural soil environments and play a significant role in various biogeochemical processes, including adsorption and redox reactions [7]. The active surface

hydroxyl sites and high adsorption capacity of Fe/Mn (hydr)oxides render them significant adsorbents [8,9]. However, natural organic matter plays a pivotal role in regulating the transport and fate of HMs within intricate geochemical cycles as crucial environmental carriers by forming colloids with Fe/Mn (hydr)oxides.

The binding of Fe and Mn to natural organic matter (NOM) in environmental media has been widely observed at the anoxic–aerobic interface [10–12]. This interaction between NOM and Fe/Mn can regulate the morphology, toxicity, and transport of trace metals, leading to the formation of colloidal Fe and Mn species [13–16]. Humic acid (HA), a typical NOM in the soil environment, contains carboxyl and hydroxyl functional groups that preferentially form stable complexes with Fe^{3+} and Mn^{2+} [17]. For example, Liao et al. [18] demonstrated that the formation of colloidal HA–Fe species controls the fate and transport of metallic chromium, while Zhang et al. [19] revealed the crucial role played by Mn(III)–HA colloids in mediating As(III) fixation by Mn. The interactions between HA and Fe/Mn (hydr)oxides are crucial in determining the formation, transport, and stabilization of HA–Fe/Mn colloids, which play a pivotal role in influencing the fate of organic compounds and metals within the global carbon cycle. Therefore, comprehending the underlying mechanism governing the interaction between HA and Fe/Mn (hydr)oxides holds significant environmental importance.

In this study, we systematically investigated the interaction mechanism governing the formation, migration, and stability of HA–Fe/Mn colloids in environmental matrices. The reaction mechanism between HA and Fe/Mn, as well as the impact of colloid formation, was substantiated by adjusting the molar ratios between C and Fe/Mn. Subsequently, a series of characterization techniques were employed to further authenticate the nature of the colloid and elucidate its formation mechanism. Furthermore, the migration behavior of HA–Fe/Mn colloids in natural environments was elucidated at the molecular level by simulating porous media using a quartz crystal microbalance with dissipation monitoring (QCM–D). Finally, the enhanced stability of the formed HA–Fe/Mn colloids in environmental media was determined. This study provides valuable insights to elucidate the binding mechanism of HA with Fe/Mn and predicts the environmental fate of the colloidal phase formed by HA–Fe/Mn, thus offering new perspectives on metal control strategies using Fe–Mn oxides as environmental carriers.

2. Materials and Methods

2.1. Materials

Humic acid (HA) was purchased from Yuanye Technology and represents the typical NOM of terrestrial origin [20,21]. The fluorescence spectra results are presented in Figure S1. 2-[4-(2-hydroxyethyl)piperazin-1-yl] ethanesulfonic acid ($C_8H_{18}N_2O_4S$) was purchased from Shanghai Aladdin Biochemical Technology Co., Ltd. (Shanghai, China). Phytic acid (H_2SO_4, 99%), nitric acid (HNO_3, 70%), hydrochloric acid (HCl, 36%), sodium hydroxide (NaOH), ferrous sulfate ($FeSO_4 \cdot 7H_2O$), and calcium chloride ($CaCl_2$) were commercially available from Sinopharm Chemical Reagent Co., Ltd. (Shanghai, China). Magnesium chloride ($MgCl_2$) and sodium chloride (NaCl) were purchased from Shanghai Macklin Biochemical Technology Co., Ltd. (Shanghai, China). Potassium permanganate ($KMnO_4$) was commercially obtained from Xilong Scientific Co., Ltd. (Guangzhou, China). All the reagent solutions were prepared using ultrapure water (resistivity >18 MΩ·cm, Milli–Q, Millipore, Shanghai, China). The chemicals utilized in this study, with the exception of HA, were all of analytical pure grade.

2.2. Formation and Characterization of HA–Fe/Mn

The HA suspensions, prepared with a concentration range of 0–50 mg C/L, were initially introduced into ultrapure water. Subsequently, the HA suspensions were supplemented with 10 mg/L of $FeSO_4$ and 10 mg/L of $KMnO_4$ to achieve a mixed solution featuring a C:Fe/Mn molar ratio ranging from 0 to 21.5. The molar ratio range of 0–21.5 was selected as it encompasses the typical C/Fe–Mn molar ratios observed in sedi-

ments [14,22,23]. The mixed solution was stirred at a speed of 400 rpm for 12 h at room temperature to generate the desired HA–Fe/Mn colloid. All the reactions were conducted in a glass reactor equipped with a lid and continuous stirring, which was shielded with aluminum foil to prevent any potential photochemical reactions. The environmentally relevant pH for all experiments was set to 7.0 and maintained at 7.0 ± 0.1 using a 5 mM solution of 4-(2-hydroxyethyl)-1-piperazineethanesulfonic acid (HEPES, ≥99.5%) buffer, chosen for its minimal impact on the interaction between HA and Fe/Mn (hydr)oxides [24,25]. All the reactors contained 5 mM NaCl, which, together with the ionic strength contributed by the HEPES, corresponds to the typical ionic strength of freshwater aquifers [26]. Due to the significant impact of background buffer (5 mM HEPES) on the accurate determination of the HA concentration using TOC analysis, NaOH and HCl were employed in lieu of HEPES to maintain the suspension's pH at 7.0 ± 0.2 using a pH titrator (Orion Star T910) for a series of experiments involving TOC measurements of the HA concentration.

In this study, the ratio of Fe to Mn ions was determined to be 3:1 based on the spatial and temporal variability in water-soluble Fe and Mn ions in soil samples collected from Lengshuijiang City, Hunan Province (27°74′ N, 111°47′ E), as outlined in the Supplementary Information (Text S2, Tables S1 and S2). A grid was established around the perimeter based on satellite images, with sampling points set up at 0.5 km intervals within a 2 km radius. Surface (0~20 cm) soil samples were collected following the Technical Specification for Soil Environmental Tests (HJ/T 166−2004). At each sampling point, five soil samples were collected and mixed in situ using an orthogonal method to obtain approximately 1 kg of soil samples.

2.3. Analytical Methods

The concentrations of Fe, Mn, and HA in soil samples from different particle size fractions were initially determined through wet chemical analysis in this study. In this context, colloids are explicitly defined as particulate matter with particle sizes ranging from 10,000 Dalton (approximately 1–3 nm) to 0.45 μm. Samples that pass through a 10,000−Dalton ultrafiltration membrane are classified as fractions in a truly dissolved state, while those retained by a 0.45 μm polyethersulfone filter membrane are considered particulate matter. The utilization of the 10,000 Dalton ultrafiltration membrane in conjunction with the 0.45 μm filtration membrane allows for precise differentiation of the authentic dissolved state Mn and HA fractions (with diameters less than 1–3 nm), the colloidal state (ranging from 1–3 nm to 450 nm in diameter), and the particulate state material (exceeding 450 nm in diameter) present within the samples.

The samples were acidified with a 2% HNO_3 solution, and the concentrations of Mn and Fe in the aqueous solution were determined using an Agilent 720ES (OES) inductively coupled plasma-optical emission spectrometer (ICP–OES) and an Agilent 7700 (MS) inductively coupled plasma mass spectrometer (ICP–MS), both from the USA. The stability of the system was evaluated using a zeta potential meter (Nano ZS, Malvern Inc., Westborough, MA, USA) during the deposition process. The morphology of the particles formed in condensation was observed using transmission electron microscopy (TEM, Talos F200S, USA), and their average size was quantified using ImageJ software version 1.54j (LOCI, 1.46r, USA). The Total Organic Carbon (TOC) was quantified using a Multi N/C 3100 Analyzer, while major components of HA were explored by collecting Excitation-Emission Matrix (EEM) data with a Hitachi F−7000 fluorescence spectrophotometer.

The HA–Fe/Mn and comparison samples were freeze-dried, and functional group analysis was conducted using Fourier transform infrared spectroscopy (FTIR, Nicolet iS50, USA). Crystallographic information was obtained through X-ray diffraction (XRD, Rigaku RINT, Japan), while changes in chemical composition were determined by X-ray photoelectron spectroscopy (XPS, ESCALAB Xi+, USA).

2.4. Aggregation of HA–Fe/Mn Colloids

The aggregation kinetics of the colloidal suspensions was investigated using time-resolved dynamic light scattering (DLS) measurements. All the light scattering experiments were conducted at a scattering angle of 90°. A complete autocorrelation function was recorded every 15 s, and DLS samples were aggregated for 20 min. The aggregation kinetics of the colloids were assessed with varying Ca^{2+} (0.5–7 mM) and Mg^{2+} (3–20 mM) concentrations. For each measurement, a suspension of HA–Fe/Mn colloids in $CaCl_2$ or $MgCl_2$ electrolyte solution at a pH of 7.0 ±v0.1 was prepared and quickly added to a polystyrene cuvette and capped. After mixing for 1.5 s, the aggregation was monitored as described above. Detailed experimental procedures and calculations are provided in Text S3 [27,28].

2.5. Colloid Deposition Kinetics

A quartz crystal microbalance with dissipation (QCM–D, QSense Analyzer) equipped with four flow cells was used to evaluate the deposition of HA–Fe/Mn colloids on the silica interface. A silica surface was chosen as the model surface because it represents an important environmental surface with properties like quartz sand. The deposition experiments were conducted following the previous literature [27]. Briefly, a HEPES/NaCl/pH 7 solution was introduced into the chamber to establish a baseline until the mean normalized third overtone tone shift no longer exceeded 0.5 Hz, stabilizing the baseline for 10 min. Next, the HA–Fe/Mn colloidal suspensions with different C/Fe–Mn molar ratios and the same electrolyte were injected into the sensor for 20 min. Changes in the frequency (Δf) and energy dissipation (ΔD) of the SiO_2−coated (5 MHz) QCM–D crystals were simultaneously monitored. The frequency and dissipation at the third overtone were used to calculate and plot for assessment of the deposited layer stiffness. Details of the experimental program are described in Text S4 [29,30].

3. Results

3.1. Inhibition of Fe/Mn (Hydr)oxide Coagulation Behavior by HA

This study examined the impact of HA concentration on the structure of Fe/Mn colloids, and Figure 1 was generated by normalizing the data presented in Table S4. The distribution of colloidal Fe/Mn content in the HA–Fe/Mn suspensions (1–450 nm) was observed to increase with the initial molar ratios of carbon and Fe/Mn (hydr)oxide interactions (C:Fe/Mn) under steady-state conditions. The presence of colloidal Fe/Mn forms gradually increased from C:Fe/Mn = 0 to higher levels (Figure 1a), reaching a maximum at a C:Fe/Mn ratio of 21.5, with percentages of 84.41% and 45.1% for Fe and Mn, respectively. With the increase in HA content, the colloidal form of Fe exhibited a significantly higher abundance compared to Mn. Commencing at C:Fe/Mn = 0, the morphological characteristics of colloidal Fe/Mn gradually increased (Figure 1a,b), reaching their peak at C:Fe/Mn = 21.5, with Fe and Mn proportions of 84.41% and 45.1%, respectively. Additionally, it is noteworthy that the abundance of colloidal Fe surpasses that of Mn as the content of humic acid increases. In accordance with the variation in Fe and Mn in different particle size fractions, the presence of colloidal HA increased proportionally to an elevated molar ratio between C and Fe/Mn (hydr)oxides (Figure 1c). Notably, a substantial amount of colloidal HA was obtained even at C and Fe/Mn molar ratios as low as 0.4. This phenomenon could be attributed to ligand exchange through the complexation between HA and soluble Fe/Mn (<1–3 nm), resulting in a reduction in the content of soluble HA [31]. Therefore, the primary factor contributing to the formation of HA–Fe/Mn colloids was the synergistic activation and complexation between HA and Fe/Mn.

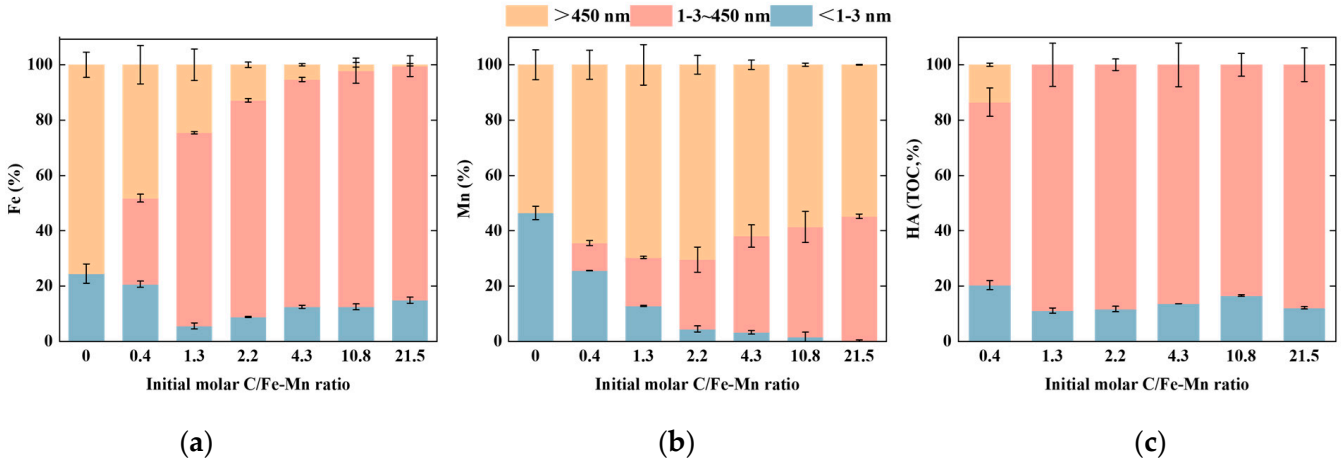

Figure 1. Particle size distribution of (**a**) Fe, (**b**) Mn, and (**c**) C in HA–Fe/Mn suspensions with varying C/Fe–Mn molar ratios.

3.2. Mechanism of HA Binding to Fe/Mn

By conducting an in-depth analysis of the FTIR data both before and after the introduction of HA, we gained comprehensive insights into the intricate mechanism underlying organic binding to Fe/Mn (hydr)oxides, thereby enabling us to determine the chemical properties exhibited by the HA–Fe/Mn colloids (Figure 2a). The FTIR spectra of the Fe/Mn (hydr)oxides exhibit significant distinctions from those of HA–Fe/Mn, indicating notable variations between the two. Prior to the reaction, a prominent adsorption band is observed at 610 cm^{-1} for Fe/Mn (hydr)oxides, which can be attributed to the metal peak, accompanied by the corresponding M–O structure. Additionally, the peak at 1108 cm^{-1} corresponds to the -OH vibrational mode of Fe/Mn (hydr)oxides [32]. After being activated and complexed by HA, the characteristic peaks of HA–Fe/Mn disappear, while COO- stretching bands at 1573 and 1380 cm^{-1} emerge, indicating the formation of metal-carboxylic acid bonds [33,34]. Therefore, in terms of HA–Fe/Mn colloid formation, the COO- functional group may serve as the primary binding site for HA to Fe/Mn (hydr)oxides, playing a crucial role in mediating interactions between natural organic matter and Fe/Mn (hydr)oxides, as well as HA–Fe/Mn colloids.

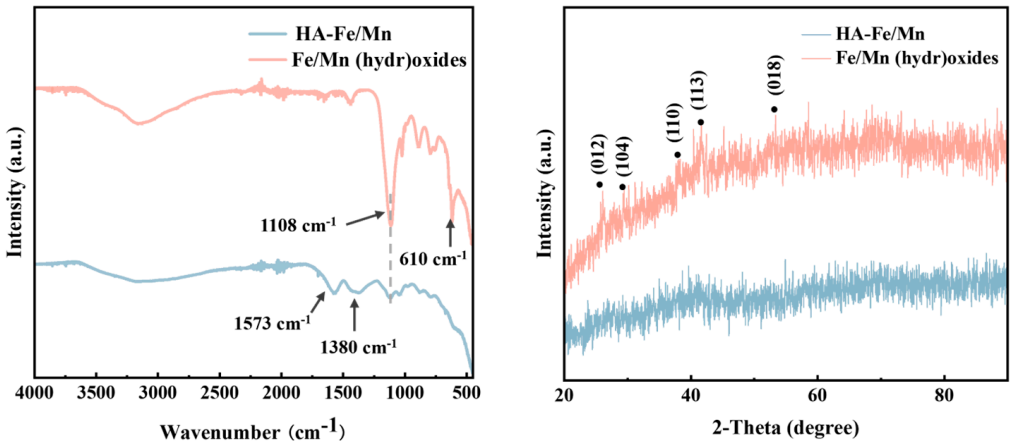

Figure 2. (**a**) FTIR results of HA–Fe/Mn and Fe/Mn (hydr)oxides and (**b**) XRD patterns of HA–Fe/Mn and Fe/Mn (hydr)oxides. FTIR analyses were performed on solid samples at a fixed initial molar C:Fe/Mn ratio of 4.3.

The structural changes following the Introduction of HA were determined by analyzing the crystal structure of the resulting HA–Fe/Mn colloids (Figure 2b). Diffraction peaks observed in the XRD spectra of Fe/Mn prior to the introduction of HA were found at 25.6°, 30.2°, 37.8°, 41.8°, and 53.3°, corresponding to (012), (104), (110), (113), and (018), respectively, which are consistent with the results obtained for Fe/Mn (hydr)oxides [35,36]. The XRD results above indicate the successful synthesis of Fe/Mn (hydr)oxides. However, due to the natural porous medium simulation in the synthesis system, the crystalline phase structure of Fe/Mn (hydr)oxides obtained at room temperature is less apparent. However, the introduction of HA did not result in the observation of characteristic peaks associated with Fe/Mn (hydr)oxides, suggesting a lack of crystallinity or an amorphous nature [28].

The choice of HA–Fe/Mn (C:Fe/Mn = 4.3) was made based on the critical stability of NOM–Fe/Mn colloids at this ratio, which was sufficient for stabilization in the medium. The morphology and distribution of HA and HA–Fe/Mn (C:Fe/Mn = 4.3) were investigated using TEM imaging, with varying molar ratios (Figure 3a–d). The microscopic morphological features of Fe/Mn (hydr)oxides and HA are depicted in Figure 3a and b, respectively. These images primarily exhibit distinct fine line structures that demonstrate a cross-linked agglomerate morphology. Microscopic morphology analysis of the HA–Fe/Mn colloid structure and distribution revealed (Figure 3c) that the introduction of HA led to an observable increase in cross-linking morphology, accompanied by enhanced dispersion, which could potentially be attributed to complexation phenomena. The structure and elemental distribution of Fe and Mn in the HA–Fe/Mn colloids were further investigated using TEM imaging and energy-dispersive spectroscopy (EDS). By analyzing the elemental distribution of Fe (Figure 3e) and Mn (Figure 3f), it is apparent that the formation of HA–Fe/Mn colloids in an HA matrix is uniformly distributed. This indicates that the presence of HA can effectively serve as a geochemical carrier for binding the elements Fe and Mn.

The Fe 2p spectra of the Fe/Mn (hydr)oxides revealed the prevalence of Fe(III) as the dominant iron species (Figure 4a). In the absence of HA, the surface ratio of Fe(III) to Fe(II) on Fe/Mn (hydr)oxides was determined to be 1.46. In contrast, the ratio of Fe(III) to Fe(II) on the HA–Fe/Mn surface is 0.82 (Figure 4c). Interestingly, the Mn 2p spectrum of HA–Fe/Mn (Figure 4d) exhibits a higher occupancy of Mn(IV) in comparison to that observed in Fe/Mn (hydr)oxides (Figure 4b). This observation suggests that the introduction of HA significantly influences the redox process between Fe and Mn, resulting in a higher proportion of Fe and Mn existing as Fe(II) and Mn(IV) [37,38]. The presence of HA as an electron acceptor in the redox reaction of Fe/Mn (hydr)oxides influences their crystallization process, thereby accounting for the observed limited crystallinity of HA–Fe/Mn colloids based on XRD characterization (Figure 2b) [39,40].

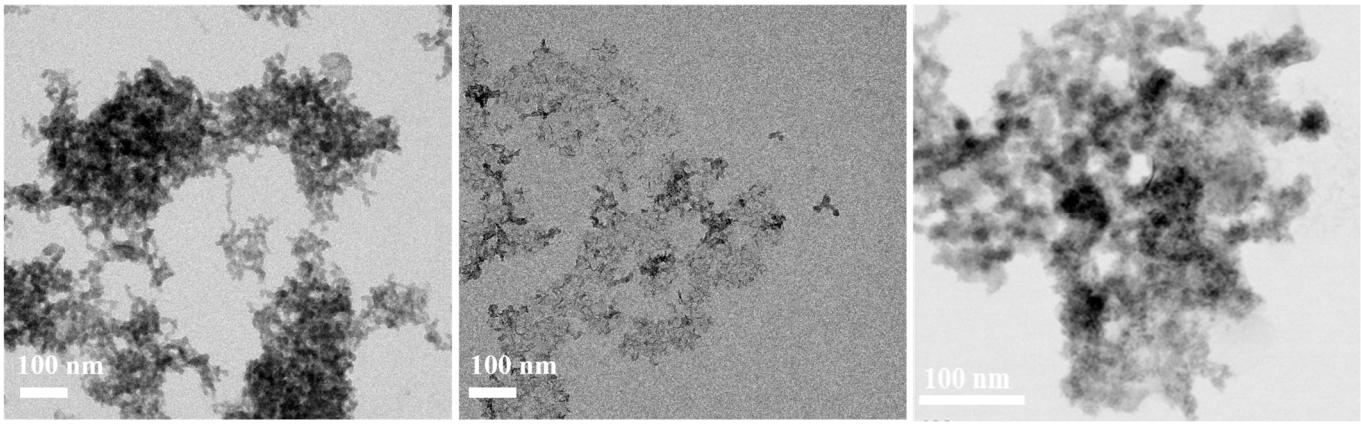

(**a**) (**b**) (**c**)

Figure 3. *Cont.*

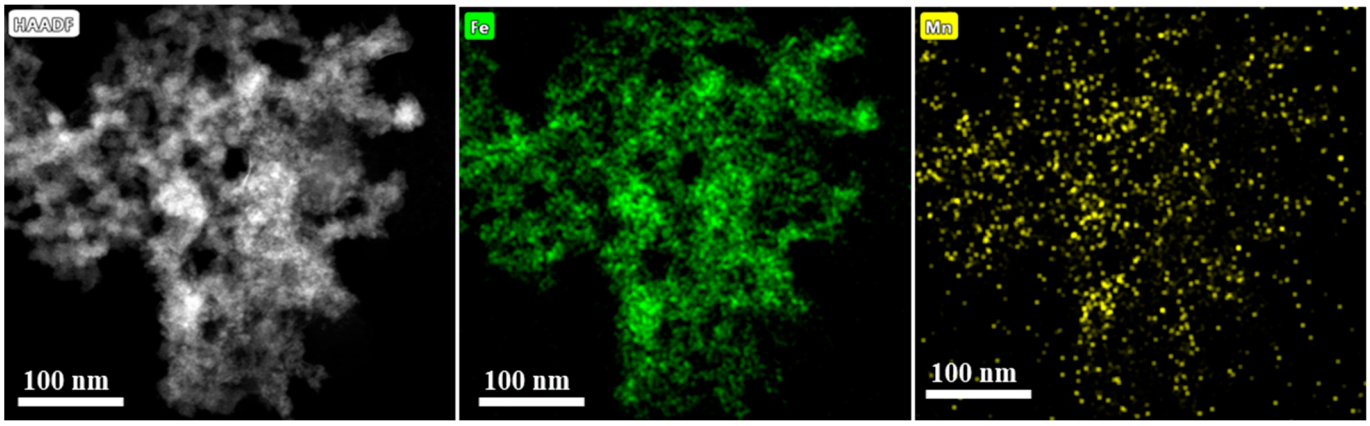

Figure 3. TEM patterns of (**a**) Fe/Mn (hydr)oxides, (**b**) HA, (**c**) HA–Fe/Mn, (**d**–**f**) TEM–EDS elemental mapping images of HA–Fe/Mn (C:Fe/Mn = 4.3).

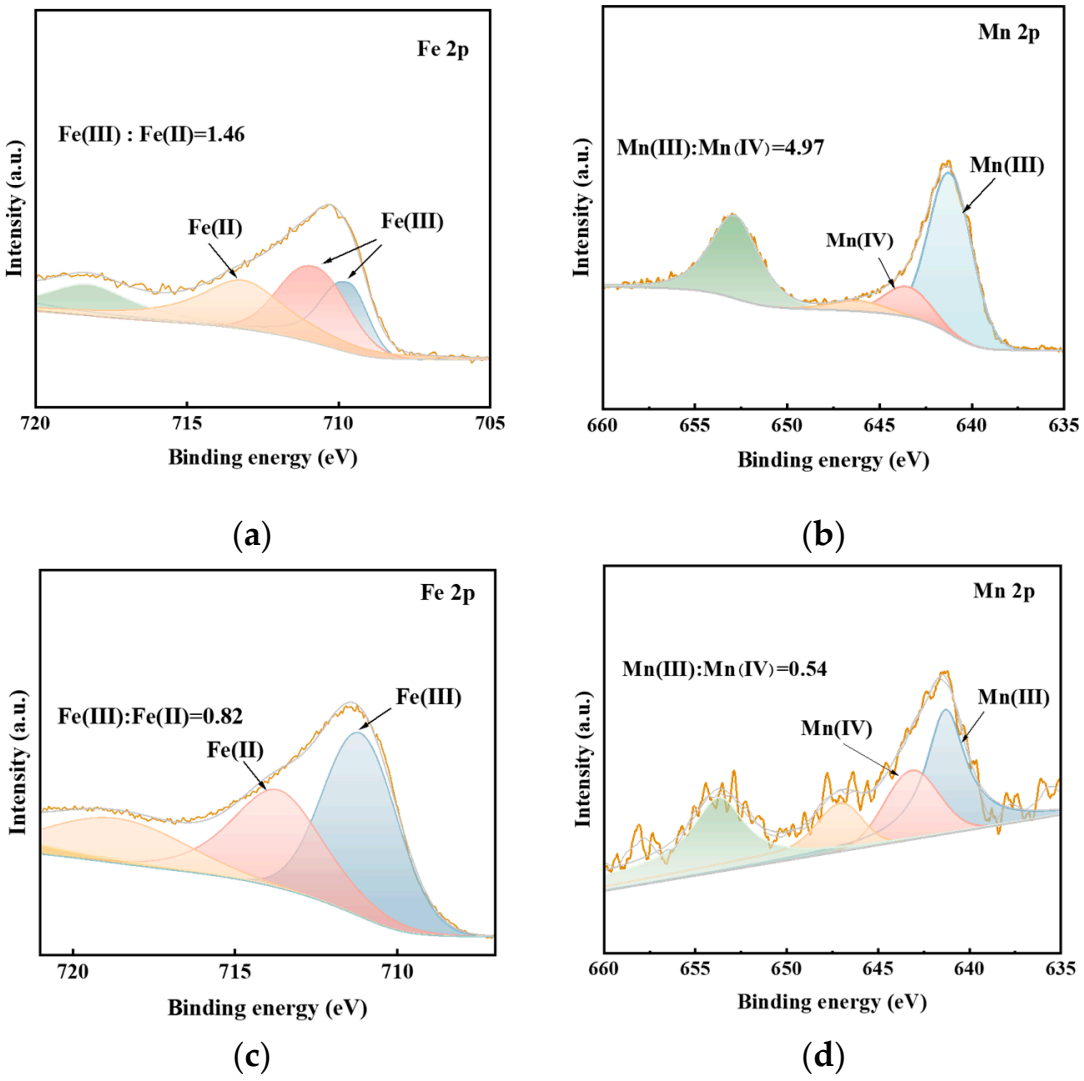

Figure 4. XPS spectroscopy. (**a**) Fe 2p and (**b**) Mn 2p spectra of Fe/Mn (hydr)oxide and (**c**) Fen2p and (**d**) Mn 2p spectra of HA–Fe/Mn. The solid samples were analyzed by XPS at a fixed initial molar C:Fe/Mn ratio of 4.3.

3.3. Microscopic Migration Mechanisms of HA–Fe/Mn Colloids

To investigate the migration behavior of the HA–Fe/Mn colloids, we utilized Ca^{2+}, Mg^{2+}, and silica sensors to simulate the actual colloid migration environment. The in situ adsorption process of the HA–Fe/Mn colloids onto silica sensors was continuously monitored in real time using QCM–D (Figure 5). Based on the temporal trend in the normalized frequency shift, it was observed that HA–Fe/Mn colloids with lower C:Fe/Mn molar ratios (concentrations below 5 mg C/L) exhibited a significant decrease in sensor frequency and reached surface saturation (equilibrium) rapidly. This was attributed to the larger particle size and higher surface potential of the HA–Fe/Mn colloids with lower C:Fe/Mn molar ratios compared to those with higher C:Fe/Mn molar ratios. At relatively high C:Fe/Mn molar ratios (concentrations exceeding 5 mg C/L), the deposition frequency of HA–Fe/Mn colloids on the sensors was found to be low, potentially due to electrostatic repulsion, which hinders the attachment of negatively charged HA–Fe/Mn colloids onto the negatively charged sensor surface in a near-neutral environment (pH 7). As a result, the deposition of HA–Fe/Mn on silica decreased as the C:Fe/Mn molar ratio increased due to the presence of natural organic matter. The results of this study confirm that the migratory properties of Fe/Mn (hydr)oxide colloids at the quartz interface are significantly enhanced when the concentration of HA exceeds 5 mg C/L, providing information on the migration of these particles in porous media where no significant attachment occurs.

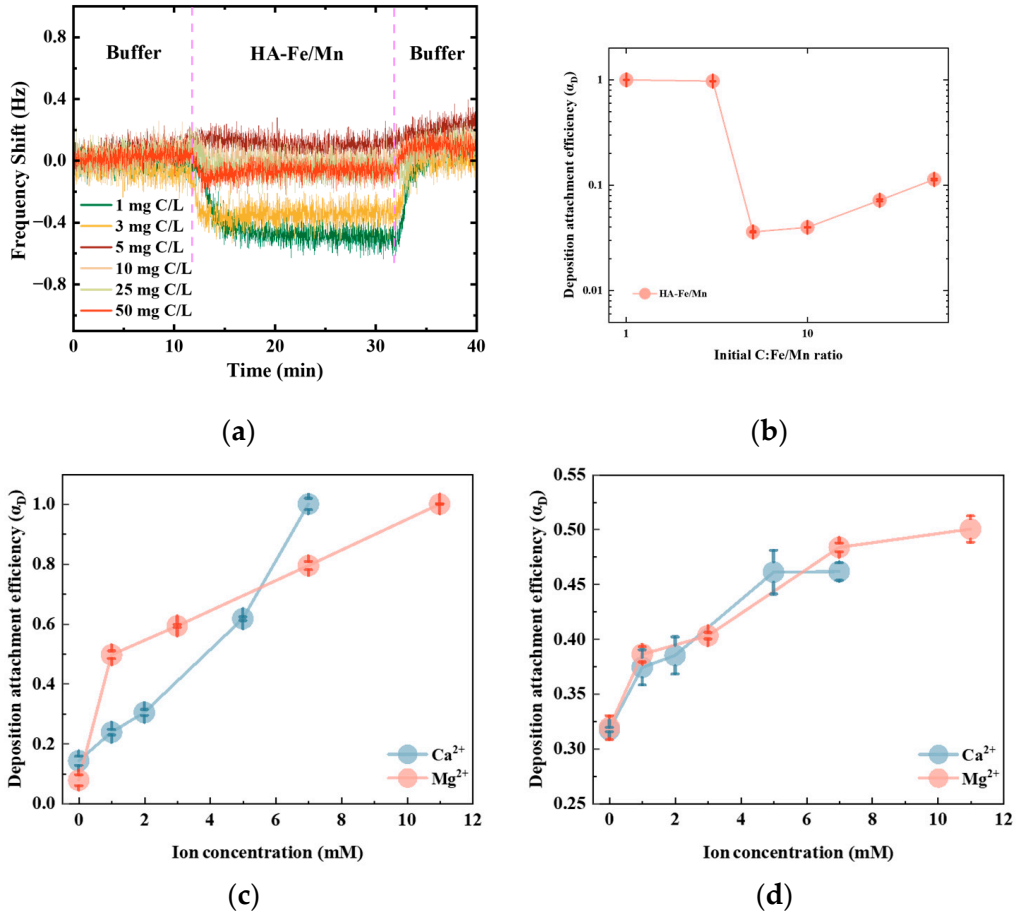

Figure 5. Normalized frequency shifts at the third overtone of (**a**) HA–Fe/Mn colloids deposited on the silica surface under pH 7 conditions and (**b**) attachment efficiency of HA–Fe/Mn colloids deposited on the silica surface. (**c**) The deposition adhesion efficiency of HA–Fe/Mn colloids on the silica surface in the presence of Ca^{2+} and Mg^{2+}. $|\Delta D(3)/\Delta f(3)|$ for (**d**) the deposition of HA–Fe/Mn colloids on the silica surface in the presence of Ca^{2+} and Mg^{2+}.

The deposition rates were investigated under realistic migration conditions, simulating the presence of calcium and magnesium cations. It was observed that the deposition rate of HA–Fe/Mn was higher in the presence of Ca^{2+} compared to Mg^{2+} (Figure 5c). The deposition rate of Ca^{2+} ions exceeded that of Mg^{2+} ions, primarily attributed to their enhanced capacity for complex formation with the COO- layer within the colloid, thereby accelerating HA–Fe/Mn deposition. According to the Sauerbrey equation, the hardness assessment of the deposited layer was determined by calculating the slope value of energy dissipation and frequency ($|\Delta D(3)/\Delta f(3)|$), where higher values indicate lower compaction and lower values indicate greater hardness of the deposited layers (Figure 5d). This finding further supports our previous observation that under identical concentration conditions, the presence of Ca^{2+} and Mg^{2+} promotes the formation of a more compact deposition layer, facilitating the retention of HA–Fe/Mn colloids on porous media surfaces and enhancing their effectiveness in removing a wide range of heavy metals.

3.4. Aggregation and Stability of HA–Fe/Mn Colloids

The stability of the HA–Fe/Mn colloids (Figure 6a–d) was assessed by analyzing the growth data on their hydrodynamic diameters, while attachment efficiencies were determined for various concentrations of divalent electrolytes (Figure 6e–h). The molar ratio between carbon and Fe/Mn (hydr)oxides was investigated in $CaCl_2$ and $MgCl_2$ electrolyte solutions to elucidate the mechanism of HA–Fe/Mn aggregation behavior. The Der–jaguin–Landau–Verwey–Overbeek (DLVO) theory predicts the stability of colloids by quantitatively assessing the balance between the repulsive and attractive forces acting on particles. If the repulsive force exceeds the attractive force, colloidal particles will remain dispersed; conversely, if a dominant attractive force prevails, particle aggregation occurs [41,42]. The experimental results show that the observed behavior of a reaction-limited mechanism ($\alpha < 1$) at lower electrolyte concentrations and a diffusion-limited mechanism ($\alpha = 1$) at higher electrolyte concentrations suggests that the aggregation dynamics of HA–Fe/Mn colloids align with the DLVO theory. The HA–Fe/Mn colloids formed at high concentrations and Fe/Mn (hydr)oxide molar ratios (21.5) exhibit reduced tendencies to aggregate and demonstrate remarkable stability (Figure 6f). This can be attributed to the increased presence of negatively charged HA groups, resulting in enhanced interparticle repulsion and consequently a stronger dispersion stability compared to colloids formed at lower C:Fe/Mn molar ratios (4.3).

The critical condensation concentration (*CCC*) value was determined according to the intersection of reaction-limited aggregation and diffusion-limited aggregation, which represents the minimum electrolyte strength required for complete destabilization of the colloid [43]. The *CCC* values of HA–Fe/Mn in the $CaCl_2$ electrolyte solution are shown in Figure 6g, which were measured as 3.7 mM (C:Fe/Mn = 4.3) and 7.7 mM (C:Fe/Mn = 21.5), respectively. Similarly, the *CCC* values of HA–Fe/Mn in the $MgCl_2$ electrolyte solution were determined to be 7.3 mM and 14.7 mM, respectively (Figure 6f). The *CCC* value of HA–Fe/Mn was observed to increase with the molar ratio between C and Fe/Mn, indicating that a higher content of HA contributed to enhancing the stability of HA–Fe/Mn and effectively counteracted the complexation/bridging effect induced by divalent cations in subsurface environments.

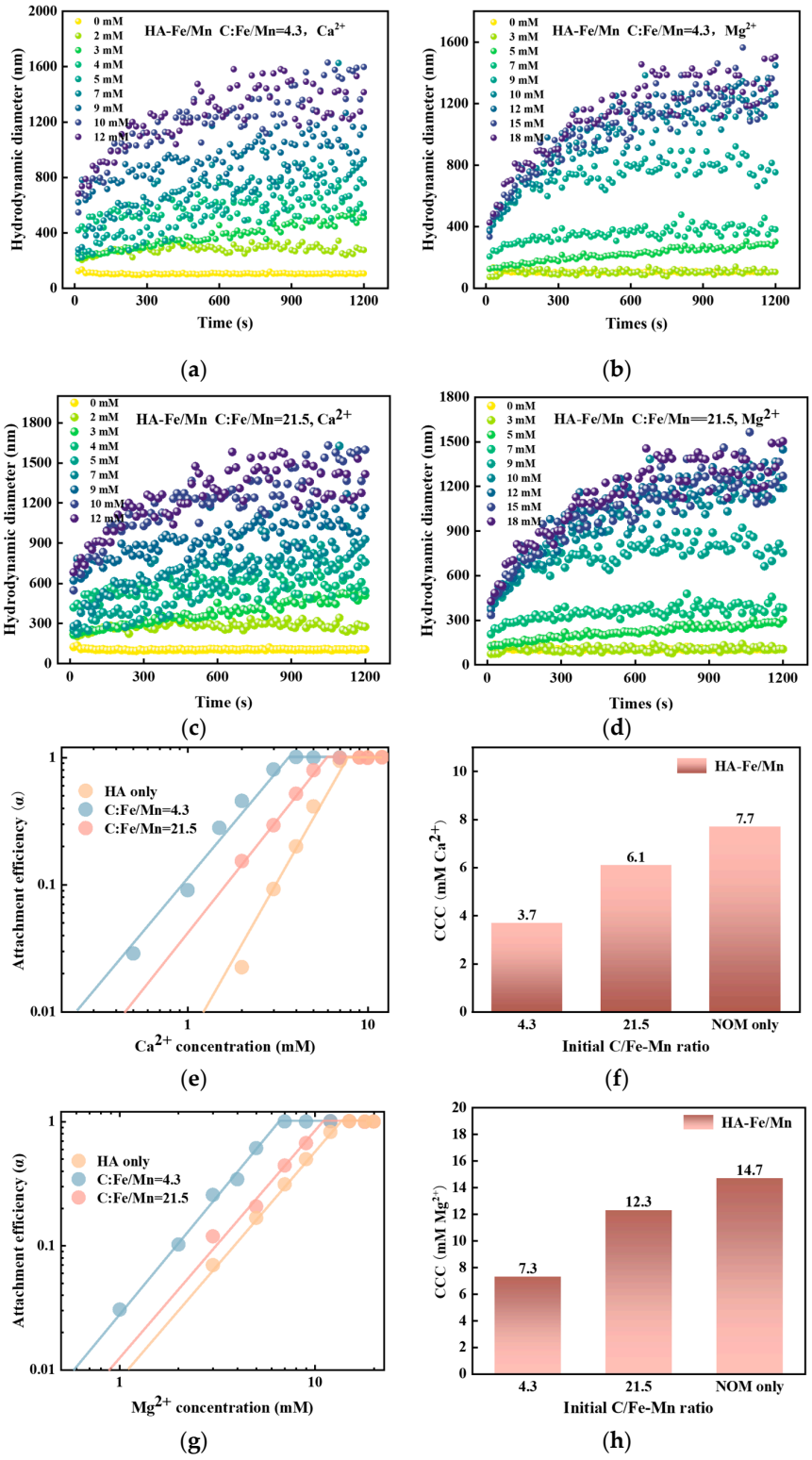

Figure 6. Representative time-resolved aggregation curves of HA–Fe/Mn colloids at different moments in (**a**,**c**) Ca^{2+} environment and (**b**,**d**) Mg^{2+} environment. Adhesion efficiency of HA–Fe/Mn colloids with different C:Fe/Mn molar ratios as a function of (**e**) Ca^{2+} and (**g**) Mg^{2+} concentrations. The corresponding critical coagulation concentrations (*CCCs*) were derived through cross-extrapolation under reaction-limited and diffusion-limited conditions, summarized in (**f**,**h**), as indicators of particle water stability.

4. Conclusions

In this study, we present findings on the formation and stability of HA–Fe/Mn colloids in porous media systems. To elucidate the mechanism underlying the interaction between humic acid and Fe/Mn (hydr)oxides, we investigated its impact on the morphological transformation of Fe/Mn (hydr)oxides. It was demonstrated that the molar ratio of carbon to Fe/Mn plays a crucial role in determining the properties of HA–Fe/Mn colloids. Higher initial molar ratios of carbon to Fe/Mn tend to enhance the formation and stability of HA–Fe/Mn colloids. Meanwhile, the redox reaction between HA and Fe/Mn (hydr) oxides induces a change in the valence states of Fe and Mn, which affects the structural features of the nanoparticles. The carboxyl functional groups on the surface of HA form a metal–carboxyl bonding structure, facilitating colloid formation. Furthermore, we quantitatively investigated the nanoscale migration behavior of HA–Fe/Mn in simulated porous media. The reaction between HA and Fe/Mn (hydr)oxides results in colloid structure formation, enabling their migration within porous media under ambient conditions while also promoting their retention within surface layers. This research provides valuable insights into important aspects related to the biogeochemical cycling of HA and Fe/Mn, as well as transport mechanisms for colloid-associated contaminants, nutrients, and trace metals in porous media.

Supplementary Materials: The following supporting information can be downloaded at https://www.mdpi.com/article/10.3390/environments11070136/s1. Figure S1: 3D fluorescence spectrum of HA.; Table S1: Summary of Batch HA–Fe/Mn Colloid Formation Experiments; Table S2: The main physicochemical properties; Table S3: Range distribution of fluorescence area integrals for HA; Table S4: Particle size distribution of HA-Fe/Mn suspensions.

Author Contributions: Conceptualization, J.Z. and W.Y.; formal analysis, J.Z.; methodology, J.Z. and W.Y.; writing—original draft, Q.L. and W.Y.; writing—review and editing, J.Z., M.J., Q.L. and W.Y. All authors have read and agreed to the published version of the manuscript.

Funding: This work was supported by Foundation for Innovative Research Groups of the National Natural Science Foundation of China (No. 52121004), National Natural Science Foundation of China (U23A20679), Key Research and Development Project of the Power Construction Corporation of China (No. DJ—ZDXM—2023—24), Hunan Provincial Natural Science Foundation (2023JJ0065).

Data Availability Statement: The original contributions presented in the study are included in the article; further inquiries can be directed to the corresponding author (yang220@csu.edu.cn).

Conflicts of Interest: The authors declare no conflict of interest.

References

1. Wang, S.; Mulligan, C.N. Enhanced mobilization of arsenic and heavy metals from mine tailings by humic acid. *Chemosphere* **2009**, *74*, 274–279. [CrossRef] [PubMed]
2. Harvey, C.F.; Swartz, C.H.; Badruzzaman, A.; Keon-Blute, N.; Yu, W.; Ali, M.A.; Jay, J.; Beckie, R.; Niedan, V.; Brabander, D. Arsenic mobility and groundwater extraction in Bangladesh. *Science* **2002**, *298*, 1602–1606. [CrossRef] [PubMed]
3. Zeng, J.; Tabelin, C.B.; Gao, W.; Tang, L.; Luo, X.; Ke, W.; Jiang, J.; Xue, S. Heterogeneous distributions of heavy metals in the soil-groundwater system empowers the knowledge of the pollution migration at a smelting site. *Chem. Eng. J.* **2023**, *454*, 140307. [CrossRef]
4. Yang, Q.; Li, Z.; Lu, X.; Duan, Q.; Huang, L.; Bi, J. A review of soil heavy metal pollution from industrial and agricultural regions in China: Pollution and risk assessment. *Sci. Total Environ.* **2018**, *642*, 690–700. [CrossRef]
5. Bjerregaard, P.; Andersen, C.B.; Andersen, O. Ecotoxicology of metals-sources, transport, and effects on the ecosystem. In *Handbook on the Toxicology of Metals*; Elsevier: Amsterdam, The Netherlands, 2022; pp. 593–627.
6. Mohammed, A.S.; Kapri, A.; Goel, R. Heavy metal pollution: Source, impact, and remedies. In *Biomanagement of Metal-Contaminated Soils*; Springer: Berlin/Heidelberg, Germany, 2011; pp. 1–28.
7. Vu, H.P.; Shaw, S.; Brinza, L.; Benning, L.G. Partitioning of Pb (II) during goethite and hematite crystallization: Implications for Pb transport in natural systems. *Appl. Geochem.* **2013**, *39*, 119–128. [CrossRef]
8. Zhang, G.; Qu, J.; Liu, H.; Liu, R.; Wu, R. Preparation and evaluation of a novel Fe–Mn binary oxide adsorbent for effective arsenite removal. *Water Res.* **2007**, *41*, 1921–1928. [CrossRef] [PubMed]
9. Szlachta, M.; Chubar, N. The application of Fe–Mn hydrous oxides based adsorbent for removing selenium species from water. *Chem. Eng. J.* **2013**, *217*, 159–168. [CrossRef]

10. Weng, H.; Yang, Y.; Zhang, C.; Cheng, M.; Wang, W.; Song, B.; Luo, H.; Qin, D.; Huang, C.; Qin, F. Insight into FeOOH-mediated advanced oxidation processes for the treatment of organic polluted wastewater. *Chem. Eng. J.* **2023**, *453*, 139812. [CrossRef]
11. Zhang, H.; Taujale, S.; Huang, J.; Lee, G.-J. Effects of NOM on oxidative reactivity of manganese dioxide in binary oxide mixtures with goethite or hematite. *Langmuir* **2015**, *31*, 2790–2799. [CrossRef]
12. Chen, J.; Gu, B.; Royer, R.A.; Burgos, W.D. The roles of natural organic matter in chemical and microbial reduction of ferric iron. *Sci. Total Environ.* **2003**, *307*, 167–178. [CrossRef]
13. Riedel, T.; Zak, D.; Biester, H.; Dittmar, T. Iron traps terrestrially derived dissolved organic matter at redox interfaces. *Proc. Natl. Acad. Sci. USA* **2013**, *110*, 10101–10105. [CrossRef]
14. Chen, C.; Dynes, J.J.; Wang, J.; Sparks, D.L. Properties of Fe-Organic Matter Associations via Coprecipitation versus Adsorption. *Environ. Sci. Technol.* **2014**, *48*, 13751–13759. [CrossRef] [PubMed]
15. Batchelli, S.; Muller, F.L.L.; Chang, K.-C.; Lee, C.-L. Evidence for Strong but Dynamic Iron-Humic Colloidal Associations in Humic-Rich Coastal Waters. *Environ. Sci. Technol.* **2010**, *44*, 8485–8490. [CrossRef]
16. Liu, L.; Yang, Z.; Zhao, F.; Chai, Z.; Yang, W.; Xiang, H.; Liao, Q.; Si, M.; Lin, Z. Manganese doping of hematite enhancing oxidation and bidentate-binuclear complexation during As(III) remediation: Experiments and DFT calculation. *Chem. Eng. J.* **2023**, *471*, 144758. [CrossRef]
17. Pokrovsky, O.S.; Manasypov, R.M.; Loiko, S.V.; Shirokova, L.S. Organic and organo-mineral colloids in discontinuous permafrost zone. *Geochim. Cosmochim. Acta* **2016**, *188*, 1–20. [CrossRef]
18. Liao, P.; Pan, C.; Ding, W.; Li, W.; Yuan, S.; Fortner, J.D.; Giammar, D.E. Formation and Transport of Cr(III)-NOM-Fe Colloids upon Reaction of Cr(VI) with NOM-Fe(II) Colloids at Anoxic-Oxic Interfaces. *Environ. Sci. Technol.* **2020**, *54*, 4256–4266. [CrossRef] [PubMed]
19. Zhang, Y.; Deng, Y.; Xue, J.; Cheng, Y.; Nie, Y.; Pi, K.; Du, Y.; Xie, X.; Shi, J.; Wang, Y. Unravelling the impacts of soluble Mn(III)-NOM on arsenic immobilization by ferrihydrite or goethite under aquifer conditions. *J. Hazard. Mater.* **2024**, *466*, 133640. [CrossRef] [PubMed]
20. Luo, W.; Zhao, X.; Wang, G.; Teng, Z.; Guo, Y.; Ji, X.; Hu, W.; Li, M. Humic acid and fulvic acid facilitate the formation of vivianite and the transformation of cadmium via microbially-mediated iron reduction. *J. Hazard. Mater.* **2023**, *446*, 130655. [CrossRef]
21. Li, W.; Li, X.; Han, C.; Gao, L.; Wu, H.; Li, M. A new view into three-dimensional excitation-emission matrix fluorescence spectroscopy for dissolved organic matter. *Sci. Total Environ.* **2023**, *855*, 158963. [CrossRef]
22. Katoh, M.; Murase, J.; Hayashi, M.; Matsuya, K.; Kimura, M. Nutrient leaching from the plow layer by water percolation and accumulation in the subsoil in an irrigated paddy field. *Soil Sci. Plant Nutr.* **2004**, *50*, 721–729. [CrossRef]
23. Chin, Y.P.; Traina, S.J.; Swank, C.R.; Backhus, D. Abundance and properties of dissolved organic matter in pore waters of a freshwater wetland. *Limnol. Oceanogr.* **1998**, *43*, 1287–1296. [CrossRef]
24. Pan, C.; Troyer, L.D.; Liao, P.; Catalano, J.G.; Li, W.; Giammar, D.E. Effect of humic acid on the removal of chromium (VI) and the production of solids in iron electrocoagulation. *Environ. Sci. Technol.* **2017**, *51*, 6308–6318. [CrossRef] [PubMed]
25. Pan, C.; Troyer, L.D.; Catalano, J.G.; Giammar, D.E. Dynamics of chromium (VI) removal from drinking water by iron electrocoagulation. *Environ. Sci. Technol.* **2016**, *50*, 13502–13510. [CrossRef]
26. Harter, T.; Wagner, S.; Atwill, E.R. Colloid Transport and Filtration of Cryptosporidium parvum in Sandy Soils and Aquifer Sediments. *Environ. Sci. Technol.* **2000**, *34*, 62–70. [CrossRef]
27. Liao, P.; Li, W.; Jiang, Y.; Wu, J.; Yuan, S.; Fortner, J.D.; Giammar, D.E. Formation, aggregation, and deposition dynamics of NOM-iron colloids at anoxic-oxic interfaces. *Environ. Sci. Technol.* **2017**, *51*, 12235–12245. [CrossRef] [PubMed]
28. Li, Q.; Xie, L.; Jiang, Y.; Fortner, J.D.; Yu, K.; Liao, P.; Liu, C. Formation and stability of NOM-Mn(III) colloids in aquatic environments. *Water Res.* **2019**, *149*, 190–201. [CrossRef] [PubMed]
29. Yan, M.; Liu, C.; Wang, D.; Ni, J.; Cheng, J. Characterization of Adsorption of Humic Acid onto Alumina using Quartz Crystal Microbalance with Dissipation. *Langmuir* **2011**, *27*, 9860–9865. [CrossRef]
30. Chen, Q.; Xu, S.; Liu, Q.; Masliyah, J.; Xu, Z. QCM-D study of nanoparticle interactions. *Adv. Colloid Interface Sci.* **2016**, *233*, 94–114. [CrossRef]
31. Oldham, V.E. *The Complexation Chemistry of Dissolved Manganese (iii) in the Ocean and Its Role in the Coupled Cycles of Carbon, Iron and Sulfur*; University of Delaware: Newark, Delaware, 2017.
32. Zhang, Y.; Yang, M.; Dou, X.-M.; He, H.; Wang, D.-S. Arsenate Adsorption on an Fe−Ce Bimetal Oxide Adsorbent: Role of Surface Properties. *Environ. Sci. Technol.* **2005**, *39*, 7246–7253. [CrossRef]
33. Sharma, P.; Ofner, J.; Kappler, A. Formation of Binary and Ternary Colloids and Dissolved Complexes of Organic Matter, Fe and As. *Environ. Sci. Technol.* **2010**, *44*, 4479–4485. [CrossRef]
34. Hay, M.B.; Myneni, S.C.B. Structural environments of carboxyl groups in natural organic molecules from terrestrial systems. Part 1: Infrared spectroscopy. *Geochim. Cosmochim. Acta* **2007**, *71*, 3518–3532. [CrossRef]
35. Hou, L.; Li, X.; Yang, Q.; Chen, F.; Wang, S.; Ma, Y.; Wu, Y.; Zhu, X.; Huang, X.; Wang, D. Heterogeneous activation of peroxymonosulfate using Mn−Fe layered double hydroxide: Performance and mechanism for organic pollutant degradation. *Sci. Total Environ.* **2019**, *663*, 453–464. [CrossRef] [PubMed]
36. Chen, G.; Nengzi, L.-C.; Li, B.; Gao, Y.; Zhu, G.; Cheng, X. Octadecylamine degradation through catalytic activation of peroxymonosulfate by FeMn layered double hydroxide. *Sci. Total Environ.* **2019**, *695*, 133963. [CrossRef] [PubMed]

37. Xiao, Z.; Yang, L.; Chen, C.; Chen, D.; Zhou, X. Redox reaction between solid-phase humins and Fe(III) compounds: Toward a further understanding of the redox properties of humin and its possible environmental effects. *J. Environ. Manag.* **2022**, *310*, 114793. [CrossRef] [PubMed]
38. Li, H.; Santos, F.; Butler, K.; Herndon, E. A critical review on the multiple roles of manganese in stabilizing and destabilizing soil organic matter. *Environ. Sci. Technol.* **2021**, *55*, 12136–12152. [CrossRef] [PubMed]
39. Colombo, C.; Palumbo, G.; Sellitto, V.M.; Cho, H.G.; Amalfitano, C.; Adamo, P. Stability of coprecipitated natural humic acid and ferrous iron under oxidative conditions. *J. Geochem. Explor.* **2015**, *151*, 50–56. [CrossRef]
40. Remucal, C.K.; Ginder-Vogel, M. A critical review of the reactivity of manganese oxides with organic contaminants. *Environ. Sci. Process. Impacts* **2014**, *16*, 1247–1266. [CrossRef] [PubMed]
41. Derjaguin, B.; Churaev, N.; Muller, V.; Derjaguin, B.; Churaev, N.; Muller, V. The Derjaguin—Landau—Verwey—Overbeek (DLVO) theory of stability of lyophobic colloids. In *Surface Forces*; Springer: Berlin/Heidelberg, Germany, 1987; pp. 293–310.
42. Tang, H.; Zhao, Y.; Yang, X.; Liu, D.; Shao, P.; Zhu, Z.; Shan, S.; Cui, F.; Xing, B. New insight into the aggregation of graphene oxide using molecular dynamics simulations and extended Derjaguin–Landau–Verwey–Overbeek theory. *Environ. Sci. Technol.* **2017**, *51*, 9674–9682. [CrossRef]
43. Chen, C.; Huang, W. Aggregation kinetics of nanosized activated carbons in aquatic environments. *Chem. Eng. J.* **2017**, *313*, 882–889. [CrossRef]